The Role of H_2O in Subduction Zone Magmatism

Timothy L. Grove,[1] Christy B. Till,[1,2]
and Michael J. Krawczynski[1,3]

[1]Department of Earth, Atmospheric and Planetary Sciences, Massachusetts Institute of
Technology, Cambridge, Massachusetts 02139; email: tlgrove@mit.edu

[2]Current affiliation: US Geological Survey, Menlo Park, California 94025

[3]Current affiliation: Department of Geological Sciences, Case Western Reserve University,
Cleveland, Ohio 44106

Keywords

volcanic arc, subducted slab, chlorite, H_2O-saturated, hydrous magma, arc
magmas

Abstract

Water is a key ingredient in the generation of magmas in subduction zones.
This review focuses on the role of water in the generation of magmas in
the mantle wedge, the factors that allow melting to occur, and the plate tec-
tonic variables controlling the location of arc volcanoes worldwide. Water
also influences chemical differentiation that occurs when magmas cool and
crystallize in Earth's continental crust. The source of H_2O for arc magma
generation is hydrous minerals that are carried into Earth by the subducting
slab. These minerals dehydrate, releasing their bound H_2O into overlying
hotter, shallower mantle where melting begins and continues as buoyant hy-
drous magmas ascend and encounter increasingly hotter surroundings. This
process is controlled by plate tectonic variables that ultimately influence the
location of the active volcanic arc above subduction zones. Water also mod-
ifies the thermodynamic properties of melts, leading to the unique chemical
composition of arc volcanic rocks and Earth's continental crust.

INTRODUCTION

For inhabitants of Earth, the occurrence of volcanic island arcs and the presence of a SiO_2-rich continental crust seems natural. But these features are truly rare on other terrestrial planets, where basalts are the dominant form of volcanic material that cover the planet's surface. On Earth, SiO_2-rich arc magmas that ultimately form the continental crust are a consequence of H_2O influencing melting in the subduction zone environment. This paper discusses the role of H_2O in magma-generation processes at subduction zones. The goal is to provide an updated view of melting from the bottom of the mantle wedge to the top of the crust of the overlying plate. We begin by discussing constraints on the pressure-temperature (P-T) conditions in the mantle wedge. We then discuss the way in which H_2O catalyzes melting in the mantle and the amount of H_2O involved in this melting process, before discussing the processes that occur when fractional crystallization takes place in the crust in the presence of H_2O. We conclude by discussing how plate tectonics influences the melting process to control the location of volcanoes in island and continental arc chains (for further details, see sidebar, Volcanic Arcs).

CONSTRAINTS ON THE PRESSURE-TEMPERATURE CONDITIONS IN THE WEDGE AND SUBDUCTED CRUST

Evidence from Primary Arc Magmas

Experimentally determined temperatures of model primary arc magmas provide the best evidence of mantle temperatures. Truly primary magmas are samples of partial-melting processes in the mantle that have been delivered to the surface without any modification by fractional crystallization. Melts that have remained unaffected by modification processes are rarely found, but primitive arc magmas that are near-primary melts are present. Primitive magmas are inferred to have Mg# > 0.7 (Mg# = Mg/[Mg + Fe^{2+}] molar) and be in equilibrium with >Fo$_{90}$ olivine in the mantle. Lavas with these characteristics have been identified in several arc settings (NE Japan, Mexico, Cascades, Indonesia, and Tonga) (Kelemen et al. 2003, Gaetani & Grove 2003, Hesse & Grove 2003, Wood & Turner 2009), but they are not commonplace. The chemical compositions of primitive, near-primary arc lavas and their experimentally determined pressures of last equilibration with the mantle and pre-eruptive H_2O contents are found in **Table 1**. One important characteristic shared by all mantle-derived melts found in arcs is that their last equilibration in the mantle appears to have occurred at ~1 GPa and 1100–1500°C, which represents conditions near the crust-mantle boundary in continental arcs. This shallow depth of equilibration provides important evidence to constrain models of mantle melting in arcs. We return to these matters in a later discussion of variations in the chemical composition and water contents of arc magmas. Another important characteristic of primitive arc magmas is their range in chemical composition from low-SiO_2 high-alumina olivine tholeiite to basaltic andesite and primitive magnesian andesite (**Table 1**), which is compositionally distinct from the more abundant andesite and dacite

VOLCANIC ARCS

Often abbreviated as arc, volcanic arc refers to a chain of volcanoes often forming an arcuate shape in map view. Such chains form at convergent tectonic-plate boundaries above a subducting oceanic plate. The volcanoes form approximately parallel to the oceanic trench, where the two plates meet, and is considered an "oceanic" or "island" arc when the overriding plate is oceanic and a "continental" arc when the overriding plate is continental.

Table 1   Chemical compositions of primitive, near-primary arc lavas

Location[a]	T[b]	P[b]	H2O[b]	SiO_2	TiO_2	Al_2O_3	FeO	MnO	MgO	CaO	Na_2O	K_2O	P_2O_5	Mg#	FeO/ MgO	Reference[c]
TGI J	1125	1.2	7.5	59.59	0.44	13.55	6.32	0.12	9.65	0.24	2.66	1.3	0.13	0.73	0.65	1
SD-438 J	1300	1.2	0	49.76	1.02	15.48	8.87	0.16	11.68	8.91	2.6	1.28	0.22	0.7	0.76	2
SH-85-41c C	1180	1	6	57.79	0.6	14.46	5.74	0.11	9.14	8.17	3.11	0.71	0.15	0.74	0.63	3
SH-85-44 C	1200	1	4.5	51.68	0.6	16.4	7.93	0.16	10.79	9.67	2.24	0.42	0.11	0.71	0.73	4
ML-82-72f C	1310	1.1	0	47.4	0.59	18.5	8.2	0.15	10.52	12.02	2.16	0.07	0.06	0.7	0.78	5
M.102 M	1300	1.7	6	49.4	0.99	14.84	7.63	0.12	11.63	8.3	3.53	1.4	0.44	0.73	0.66	6
Av-MGB I			0.3	49.1	0.82	15.9	8.9	0.17	10.5	11.3	2.21	0.34	0.1	0.68	0.85	7
BON IB	1480	1.5	2.5	51.88	0.7	8.71	8.94	0.12	20.69	7.1	1.7	0.16		0.8	0.43	8
V35-5 A				56.54	0.61	16.68	4.84	0.12	6.62	7.2	3.89	1.3	0.13	0.75	0.73	9
ID16 A	1320	1.2	0	48.9	0.7	16.01	8.9	0.17	11.42	10.89	2.21	0.52	0.12	0.7	0.78	10

[a] Key to locations: J, Japan; C, Cascades; M, Mexico; I, Indonesia; IB, Izu-Bonin; A, Aleutians.

[b] T (temperature) in °C; P (pressure) in GPa; H2O contents in weight percent (wt%).

[c] References: 1. Tatsumi (1981). 2. Tatsumi et al. (1983). 3, 4. Grove et al. (2003). 5. Bartels et al. (1991). 6. Hesse & Grove (2003). 7. Sisson & Bronto (1998). 8. Falloon & Danyushevsky (2000). 9. Yogodzinski et al. (1995). 10. Draper & Johnston (1992).

lavas that make up the bulk of island and continental arc volcanoes. We also return to a discussion of H_2O's influence on these characteristics later in the paper.

Evidence from Subducted Oceanic Crust

P-T conditions preserved in exhumed subducted oceanic lithosphere would provide the ideal evidence for the conditions where the transfer of chemical components in either fluid and/or melt takes place in subduction zones (pressure of 3 GPa or greater). Only a handful of localities are known to preserve rocks that experienced these conditions: the Western Gneiss region, Norway (Hacker et al. 2010); the Sanbagawa belt, SW Japan (Mori & Banno, 1973); and Cima di Gagnone in the Swiss Alps (Evans & Trommsdorff 1974, 1983). The Sanbagawa subduction-type metamorphic belt in SW Japan represents the deepest exposed portion of a Mesozoic accretionary complex along the Japanese island arc. Located on the island of Shikoku, the Higashi-akaishi peridotite body is the largest ultramafic lens within the Sanbagawa belt and is dominantly composed of dunite, lherzolite, and garnet clinopyroxenite, interfingered in one locality with quartz eclogite (Enami et al. 2004, Mizukami & Wallis, 2005). Previous work indicates the P-T history of the peridotite includes prograde metamorphism with peak temperatures of 700–810°C and pressures of 2.9–3.8 GPa at approximately 110–120 million years ago (Enami et al. 2004). In the Swiss Alps, rocks exposed in the Cima di Gagnone, Finero (Zanetti et al. 1999, Brouwer et al. 2005), and Alpe Arami (Brenker & Brey 1997, Paquin & Altherr 2001, Olker et al. 2003, Nimis & Trommsdorff 2001, Bocchio et al. 2004) regions hold the potential to reveal mechanisms of hydrous mantle melting. Previous work on the Gagnone metamorphic body (Evans & Trommsdorff 1974, 1983; Pfiffner & Trommsdorff 1998) indicates it experienced peak metamorphic conditions of 2.4 GPa and 800°C and contains lenses of garnet-bearing peridotite, chlorite peridotite, and eclogite folded between pelitic gneisses. Metarodingites are found in association with the eclogite and suggest at least a portion of this ultramafic body preserves a remnant of oceanic crust. The peak-metamorphic conditions of these ocean crust and mantle-wedge-related metamorphic rocks place them at a depth near the wedge–slab interface—the subducted lithosphere boundary that is below the location of volcanic arcs.

Models of the Thermal Structure of Subduction Zones

Beginning with the classic study of Toksoz et al. (1971), numerical modelers have sought to infer the physical conditions encountered when subduction of the cold oceanic lithosphere causes the flow of mantle material into and around the wedge corner and back down into the mantle. Early models reproduced the basic thermal structure, but could not recover exact conditions inferred from petrologic constraints. Models have greatly improved in the past 10 years (van Keken et al. 2002, Kelemen et al. 2003, Cagnioncle et al. 2007) and now predict mantle wedge conditions that approach those inferred from the petrologic evidence (**Figure 1**). Notable progress has been achieved by understanding the depth at which coupling occurs between the subducted slab and the mantle wedge (e.g., Wada & Wang 2009) and by implementing more sophisticated models of temperature-dependent rheology in mantle flow (e.g., van Keken et al. 2008). Syracuse et al. (2010) developed a comprehensive model that spans the global variability in subduction zone physical parameters and predicts the thermal structure of the wedge-lithosphere systems. The temperatures predicted at the base of the mantle wedge (specifically the mantle directly above the interface between the wedge and the subducted oceanic lithosphere) from these models are also shown in **Figure 1**. Here we use the results of these new models of P-T conditions in the mantle wedge and subducted lithosphere to discuss the petrologic controls on melting involving water.

Metarodingite: a metamorphosed and/or metasomatized rodingite, which is an altered oceanic basalt that tends to be rich in grossular garnet and calcic pyroxene enveloped in serpentinite

Slab: a subducting oceanic plate composed of sediment, basaltic oceanic crust, and lithospheric mantle as well as the aqueous alteration of these constituents
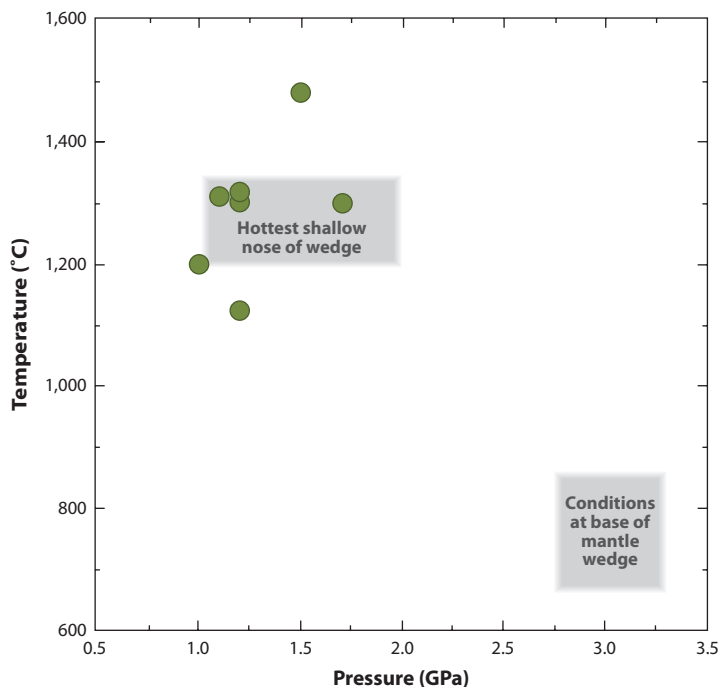
Figure 1

Pressure-temperature diagram comparing the conditions of the last equilibration with the mantle of near-primary arc magmas (*green dots*; see **Table 1**) and the range of temperatures and pressures predicted by models of the physical processes occurring in the mantle wedge in arc environments (*gray boxes*). The field labeled "Hottest shallow nose of wedge" is the part of the wedge where the highest hydrous flux melting temperatures are reached (e.g., to the backarc side of path B in **Figure 6a** labeled HNW). "Conditions at base of mantle wedge" refers to the temperature at the contact between the subducted oceanic lithosphere and the overlying mantle wedge (e.g., base of dashed line in **Figure 6a**) where fluid-fluxed melting is occurring.

MELTING PROCESSES IN THE ARC MANTLE

It is generally agreed that melting in subduction zones is initiated in the mantle wedge above the subducted oceanic lithosphere due to an influx of volatiles (Gill 1981, Tatsumi et al. 1986, Davies & Stevenson 1992, Gaetani & Grove 2003). We propose that this melting occurs at low temperatures when a small amount of H_2O-rich fluid causes the first melt to be generated at the vapor-saturated solidus (P1,T1 in **Figure 2**). However, no consensus exists regarding the specific nature and location of this melting process.

In contrast, mantle melting beneath mid-ocean ridges occurs by adiabatic decompression under anhydrous conditions (Klein & Langmuir 1987, Asimow et al. 2001) (**Figure 2**) (anhydrous adiabat). Because the adiabat has a shallower slope than does the dry peridotite solidus, upwelling mantle intersects and crosses the solidus and obtains the heat of fusion by cooling from the adiabat to the melting curve. This process has been proposed to operate in the subduction environment (Tatsumi et al. 1983, Nye & Reid 1986, DeBari et al. 1987, Plank & Langmuir 1988), and there are examples of near-anhydrous melts that have been generated in subduction zones (Tatsumi et al. 1983, Bartels et al. 1991, Sisson & Bronto 1998, Elkins-Tanton et al. 2001) by mantle that is transported into the mantle wedge by corner flow (Wiens et al. 2008).

Mechanisms other than adiabatic decompression melting are required to form hydrous magmas. For example, in hydrous-flux melting, incipient melting begins near the base of the mantle

H_2O- or vapor-saturated: describes a liquid that is in equilibrium with water in excess of that which can be dissolved in the liquid

Anhydrous: lacking H_2O
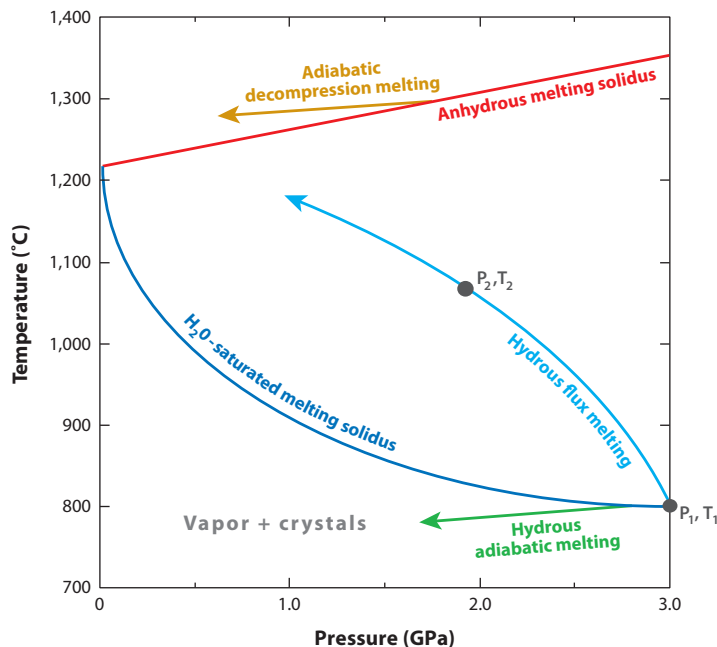
Figure 2

This pressure-temperature diagram shows three styles of mantle-melting processes. The anhydrous (*red line*) and H_2O-saturated (*dark blue line*) melting solidi for peridotite are shown. In adiabatic decompression melting under anhydrous conditions (*orange arrow*), the melt and mantle cool as they ascend to shallower depths. Melting by this mechanism, if it involved a vapor-saturated first melt on the H_2O-saturated solidus, would crystallize the melt and place it in the vapor + crystals field. Hydrous flux melting (*light blue arrow*) can occur in the mantle wedge because the temperature increases above the slab-wedge interface. A vapor-saturated melt (*light blue arrow*) produced by this process ascends into shallower hotter mantle and comes into thermal and chemical equilibrium by increasing temperature and melt fraction. After Gaetani & Grove (2003).

wedge in the presence of a small amount of H_2O derived from the slab or wedge, because the presence of H_2O depresses the peridotite solidus. If this melt and its matrix were to ascend into the overlying wedge along an adiabatic gradient, it would enter the crystal plus vapor field and freeze (**Figure 2**, hydrous adiabat) within the mantle wedge (Nicholls & Ringwood 1972, Tatsumi & Eggins 1995). When excess H_2O is present, melting can continue only if the ascending mass is small enough that it can be thermally equilibrated by the surrounding hotter mantle and heat can be transferred into it to drive a melting process. Potential melting mechanisms that would allow this to happen include the following: (*a*) the development of small diapirs of less dense, partly molten mantle that rise into the mantle wedge and further melt as they decompress (Tatsumi et al. 1983, 1986; Kushiro 1990; Pearce et al. 1995) or (*b*) a reactive porous-flow process (Kelemen 1986; Kelemen et al. 1990; Grove et al. 2002, 2006). In reactive porous flow (labeled hydrous flux melting in **Figure 2**), a buoyant H_2O-rich melt percolates up through the mantle wedge and reacts with and dissolves the surrounding mantle, thus decreasing the relative abundance of H_2O in the melt.

When solid mantle and a small amount of H_2O-rich fluid are heated to temperatures in excess of the vapor-saturated solidus, melt is generated (P_1, T_1, **Figure 3**). This first melt is extremely rich in H_2O ($\sim$30 wt%) (Hodges 1974, Mysen & Boettcher 1975) and will be positively buoyant
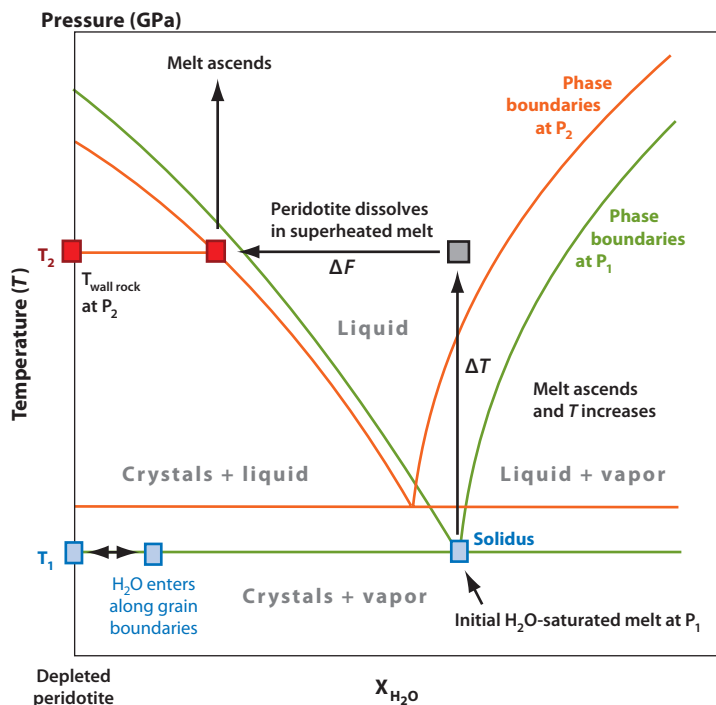
Figure 3

A polybaric temperature-composition phase diagram that illustrates the process of hydrous flux melting of the mantle wedge by reactive porous flow or by ascent of small, but buoyant, low-viscosity diapirs of mantle plus melt. The temperature-pressure path followed during this melting process is shown in **Figure 2** as "Hydrous flux melting" and the melting relations for two pressures are shown. At P_1, T_1, melting begins at the vapor-saturated solidus. This fluid-saturated melt ascends to shallower depths (P_2, T_2) in the inverted temperature gradient of the mantle wedge, where it is out of equilibrium with its surrounding mantle. The melt contains more H_2O than does an equilibrium melt at the same temperature, and the melt dissolves the surrounding mantle, increasing melt fraction and decreasing melt H_2O content. Modified after Grove et al. (2002).

and percolate upward by porous flow. At these shallower, hotter conditions, the melt will be vapor undersaturated and superheated with respect to the vapor-saturated solidus, placing it out of equilibrium with its surroundings. The melt will thus tend to dissolve the surrounding silicate minerals in the peridotite and approach chemical and thermal equilibrium causing the H_2O content of the melt to decrease (ΔF) (**Figure 3**) until it reaches the equilibrium concentration of the vapor-undersaturated liquid-solid boundary at (P_2, T_2). This process will continue as the melt ascends to shallower depths and encounters progressively hotter peridotite. In this porous-flow model, the melt composition and H_2O content are dictated by the last depth of equilibration.

Models of diapiric flow have also been proposed (Hall & Kincaid 2001). In these models, slab rollback leads to three-dimensional mantle-flow patterns and the development of diapirs that ascend into the hotter mantle and can be melted. Melts generated through this mechanism are likely to be batch melts that re-equilibrate with the diapir mass as they ascend. By contrast, in reactive porous-flow, the ascent velocity of the melt and the permeability of the mantle will exert controls on the time that melt and mantle remain in contact and thus effect the composition of melts formed (Grove et al. 2002).

MANTLE PHASE EQUILIBRIA

Peridotite-H_2O Melting

Between 1968 and 1975, four experimental studies reported on the melting of peridotite under H_2O-saturated and upper-mantle pressure conditions (Kushiro et al. 1968, Green 1973, Millhollen et al. 1974, Mysen & Boettcher 1975). These studies were revisited by Kawamoto & Holloway (1997) and more recently by Grove et al. (2006), Green et al. (2010), and Till et al. (2011), and a thermodynamic model of H_2O-saturated melting was presented by Smith & Asimow (2005). The P-T conditions of H_2O-saturated melting in the early work fell into one of two groups depending on the duration of the experiment. Shorter experimental durations (<3 h) found solidus temperatures of ~1000°C at 3 GPa while longer experimental durations (24–64 h) yielded solidus temperatures of ~800°C at 3 GPa. Grove et al. (2006) and Till et al. (2011) investigated the melting of a fertile peridotite composition and reported a low-temperature solidus (**Figure 4**) (800°C at 3 GPa) similar to that obtained by Mysen & Boettcher (1975). Green et al. (2010) reported that melting begins at a higher temperature (1100°C at 3 GPa) (**Figure 5**) similar to their earlier work (Green 1973). The difference between the two studies lies in the interpretation of what constitutes the first melt. As the diagnostic criterion for the presence of quenched hydrous
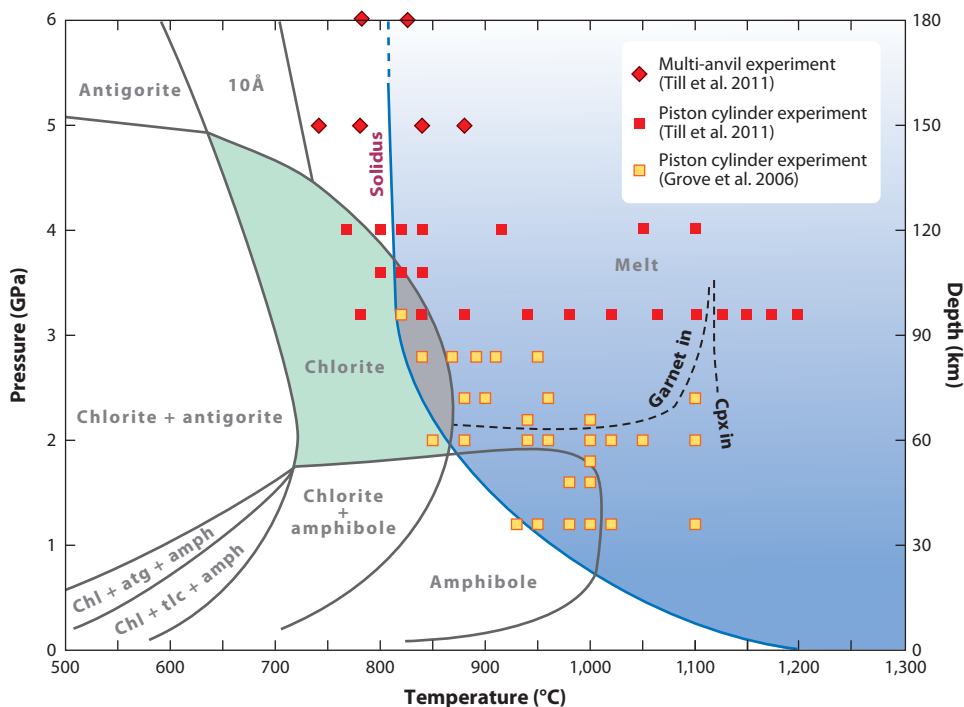
Figure 4

Experimentally determined phase diagram for H_2O-saturated peridotite from Grove et al. (2006) and Till et al. (2011). Experiments were conducted with the primitive mantle composition of Hart & Zindler (1986). Hydrous and aluminous phase stabilities that are not constrained by the experiments conducted by Grove et al. (2006) and Till et al. (2011) are derived from Ulmer & Trommsdorff (1995), Fumagalli & Poli (2005), and Pawley (2003). Abbreviations: amph, amphibole; atg, antigorite; Chl, chlorite; Cpx, clinopyroxene; tlc, talc.

silicate melt in an experiment, Green (1976) and Green et al. (2010) use the presence of interstitial patches of amphibole and/or quench clinopyroxene, mica, and glass all with Mg# of 70–85 within the experiment. Conversely, the lack of mafic silicates in the quench material is interpreted as a quench of a subsolidus vapor phase (see sidebar, Quench Material). Till et al. (2011) show that above 800°C at 3–4 GPa, and until 1100°C at 3 GPa, the Mg# of crystalline phases changes in a manner that is consistent with solid-melt partitioning rather than solely solid-fluid partitioning. Thus, the differences in the two interpretations might be a matter of semantics, and can be resolved once the "melt" or "fluid" compositions are directly analyzed.

Hydrous Mineral Phase Stability

Chlorite is stable to temperatures just above the H_2O-saturated solidus between 2 and 3.6 GPa (Pawley 2003, Fumagalli & Poli 2005, Grove et al. 2006, Till et al. 2011, Dvir et al. 2011) (**Figure 4**). Above 3.6 GPa, the H_2O-saturated solidus and the chlorite stability fields diverge. Chlorite contains ~13 wt% H_2O in its structure, and a fertile peridotite has enough Al_2O_3 to stabilize 6–7 wt% chlorite. This translates to ~2 wt% bulk H_2O in meta-peridotite at the P-T conditions of the vapor-saturated solidus. Schmidt & Poli (1998) and Grove et al. (2006) noted that
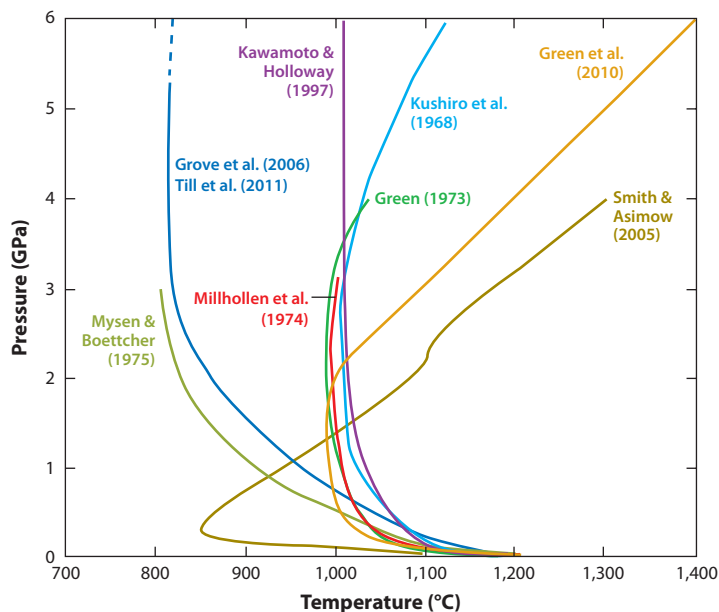
Figure 5

Experimental and theoretical determinations of the H_2O-saturated peridotite solidus.

chlorite is a stable mineral in the P-T range appropriate for the base of the upper mantle wedge. Chlorite, as well as serpentine, likely form in the shallow part of the slab-wedge interface from fluids released during the dehydration of serpentine and amphibole in the subducting oceanic crust and lithosphere (Schmidt & Poli 1998, Iwamori 1998, Pawley 2003, Grove et al. 2006, Iwamori 2007) or from H_2O produced by the dehydration of subducted sediments. Seismic images of the Honshu subduction zone reveal a low-velocity layer that is interpreted to reflect the presence of hydrous phases in the shallow wedge (Kawakatsu & Watada 2007). Thus hydrous phases, such as chlorite and serpentine, can be exposed to downward transport in the mantle wedge by corner flow.

Chlorite in fertile peridotite will breakdown at temperatures above the H_2O-saturated solidus at 800 to 820°C over the pressure range of 2 to 3.6 GPa (**Figure 4**). Structural water released from chlorite can trigger melting of the mantle and/or perpetuate H_2O-saturated melting previously initiated by H_2O fluxing following the breakdown of other hydrous phases in the subducting mantle lithosphere. We suggest that H_2O is fluxed into the base of the mantle wedge from the dehydration of phases in both the underlying subducted slab and the base of the mantle wedge (**Figure 6a**). The existence of chlorite in the mantle wedge at temperatures 100–150°C higher than serpentine dehydration assures that H_2O is available at the H_2O-saturated solidus at subarc

Hydrous phase: a mineral or melt that contains hydrogen as an essential structural constituent. In the mineral it is usually incorporated as hydroxyl (OH^-) groups
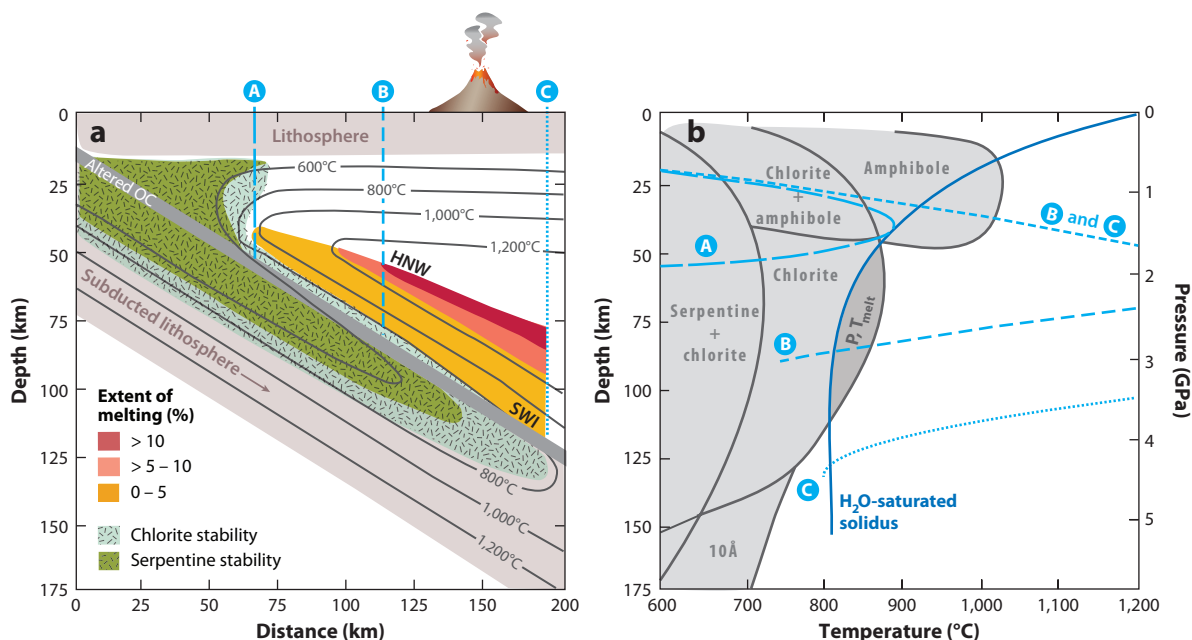
Figure 6

Two diagrams that schematically illustrate the conditions that limit hydrous flux melting in subduction zones. (*a*) A typical cross section through a subduction zone using the thermal model from Grove et al. (2009) for a slab dip of 30° and a convergence rate of 40 km per million years. Also shown are the stability limits for high-H_2O (>10 wt%) minerals. The melting model from Grove et al. (2006) is used to predict the extents of hydrous flux melting in the bottom half of the wedge. HNW denotes the hottest, shallowest nose of the mantle wedge where the maximum amount of melting occurs. The part of the mantle wedge directly above the interface between subducted oceanic lithosphere and the mantle is denoted SWI and extends from path A to path C. (*b*) Phase diagram from **Figure 4** with the temperature-depths paths from panel *a* superimposed. The dark gray region labeled P,T_{melt} shows the region of pressure-temperature space where the stability of hydrous phases in the base of the mantle wedge allows H_2O-saturated melting to begin. Figure with minor modifications from Grove et al. (2009). Abbreviations: HNW, hot nose of the wedge; OC, oceanic crust; SWI, slab-wedge interface.

depths. Therefore, the presence of chlorite in the wedge provides a mechanism for transporting significant quantities of water (up to 2 wt% H_2O in bulk peridotite) into the mantle, even in hot subduction zones, and removes the need for anhydrous slab melting in hot-slab environments, where the slab is thought to have lost water and must heat up to a much higher temperature before it can melt. Sources of H_2O will be present in minerals above and below the subducted oceanic crust.

The maximum depth stability of hydrous minerals, and thus the maximum depth at which water released within the slab is released into the overlying mantle wedge, is influenced by the temperature structure in the subducted lithosphere (**Figure 6a**). In addition to chlorite, serpentine and the 10-Å phase are two hydrous minerals that are stable to considerable depths in the subducted oceanic lithosphere (up to 150 km, depending on the P-T structure of the slab) (Iwamori 1998, Pawley 2003, Fumagalli & Poli 2005). Amphibole was once proposed as a carrier for transporting water to depth in the mantle (Wyllie 1982, Davies & Stevenson 1992), but the depth to the slab beneath arc volcanoes is beyond the high-pressure stability of amphibole. As shown in recent vapor-saturated peridotite melting experiments (Grove et al. 2006, Médard & Grove 2006, Till et al. 2011), amphibole is stable from ∼0.8 to 2 GPa on the solidus, and chlorite is stable from 2 to 3.6 GPa (**Figure 6b**), although uncertainty remains about whether the experimental bulk-water content affects amphibole stability (Green et al. 2010).

Once low-extent H_2O-rich melts are formed in the mantle wedge near the slab-wedge interface and ascend buoyantly into the mantle wedge, the next important petrologic control on mantle melting at subduction zones is the temperature structure in the overlying mantle wedge. In **Figure 6**, melting processes in the overlying wedge are illustrated by selecting three P-T paths through the region where the mantle will be saturated with an H_2O-rich fluid and/or it will be hot enough to begin melting at the vapor-saturated peridotite solidus. In path A, the hottest part of the mantle wedge is at the vapor-saturated solidus, and melting can occur because of the breakdown of several hydrous minerals in the subducted lithosphere. However, as soon as that melt separates and ascends into the overlying cooler mantle, it will freeze because the P-T path drops below the vapor-saturated solidus. For path B, an H_2O-rich fluid is supplied by the breakdown of chlorite from the underlying subducted lithosphere, and melting begins at the vapor-saturated solidus. We propose that the amount of melt produced will be limited by the amount of H_2O added and that, generally, the supply of H_2O will be a limiting factor in melting. This initially vapor-saturated melt will ascend into the overlying, hotter, shallower mantle wedge and undergo flux melting as it equilibrates with ambient temperature conditions. It will then follow a vapor-undersaturated melting path through P-T space (described above and illustrated in **Figure 2**). As the melt ascends into shallower mantle, it reacts and dissolves solid minerals, increasing the amount of melt and lowering the H_2O content of the melt (**Figure 6a** shows a melting model from Grove et al. 2006). The amount of melting in a vertical column depends on the maximum temperature achieved in the hottest part of the mantle wedge and on thermal equilibration between melt and surrounding mantle, and the extent of melting will increase for vertical paths that are farther from the wedge corner. In path B, the maximum temperature and the maximum amount of melting will occur in the hot core of the wedge, and the melt will then ascend into the cooler, shallower mantle above and ultimately into the crust.

For ascent paths further away from the wedge corner (path C, **Figure 6**), H_2O—the essential ingredient to producing vapor-saturated melting—will ultimately be exhausted as the subducted lithosphere and lower part of the mantle wedge warm to temperatures above the maximum stability temperature and pressure of hydrous minerals (there are other hydrous minerals that remain stable, but their abundance is low). The absence of H_2O-bearing minerals terminates vapor-saturated melting (path C, **Figure 6**). Thus, melting is possible over a region above the slab between path

A and path C that is defined by the temperature structure in the wedge and the supply of H_2O from the lithosphere and lower part of the mantle wedge.

The above discussion is a simplified explanation that focuses on the P-T constraints from phase equilibria. There are other important variables that need to be considered, including the permeability of the mantle and available pathways for fluid and melt ascent in the mantle wedge. Mibe et al. (1999) demonstrated that the permeability of an olivine-rich peridotite varies with pressure and temperature in the mantle wedge and that fluid can ascend into the wedge and allow melting to begin only when the grain-boundary geometry changes to produce an interconnected, permeable network. Cagnioncle et al. (2007) proposed that mantle flow and temperature structure in the overlying wedge can deflect the ascent paths of melt as it ascends into the overlying wedge, and Hall & Kincaid (2001) suggested that diapiric flow and the establishment of melt channels may influence the ascent of melt in the wedge. We return to these models in the last section of this review where we determine the extent to which the variability in the location of arc volcanoes can be explained by the supply of water, temperature structure, and kinematic variables associated with subduction.

COMPOSITIONS OF MAGMAS IN SUBDUCTION ZONES

In the Introduction, we highlight the uniqueness of Earth's SiO_2-rich continental crust, which, on average, is thought to have the composition of andesite (Rudnick & Fountain, 1995). The presence of magmatic H_2O appears responsible for this SiO_2 enrichment in two ways: (*a*) The processes of hydrous mantle melting can lead to the direct production of andesitic primary magmas, and (*b*) fractional crystallization of H_2O-bearing melts influences the mineral phase appearance sequence in basaltic and andesitic primary magmas leading to the production of SiO_2-rich continental crust. Both processes produce mafic residual products from intracrustal fractional crystallization that must be returned into the mantle by some process. A mechanism that can return these mafic cumulates to the mantle is lower crustal delamination (Kay & Kay 1993, Rudnick 1995), whereby mafic cumulates sink into the lower crust and return to the convecting mantle. We suggest that these water-controlled mechanisms are the dominant ones that produce SiO_2-rich continental crust, but there are other ways to make andesite and dacite melts. For example, assimilation of SiO_2-rich material by hot anhydrous basaltic magma during crystallization in the crust (DePaolo 1981, Grove & Kinzler 1986) and melting of hydrated basaltic crustal materials (e.g., amphibolite) (Rushmer 1991, Sen & Dunn 1994, Rapp & Watson 1995) can also produce SiO_2 enrichment in magmas.

MANTLE-MELTING CONTROLS

An examination of **Table 1** documents that near-primary arc magmas are sometimes basaltic in composition and may be either dry or H_2O rich. Melting experiments on mantle peridotite at H_2O-undersaturated conditions leads to the production of melts that fall within the basalt compositional range (Kushiro 1990, Hirose & Kawamoto 1995, Hirose 1997, Gaetani & Grove 1998, Parman & Grove 2004). These mantle melts resemble primary anhydrous melts of mantle lherzolite, but they differ in several important characteristics. These experimentally produced melts are characterized by higher $SiO_2/(MgO+FeO)$, and the presence of 3 wt% H_2O in the melt increases SiO_2 in the melt by 1 wt% (melt composition recalculated without H_2O) (Gaetani & Grove 1998). Additionally, evidence for the involvement of H_2O in arc magma melt generation is manifested in the mineral-melt partition coefficients (e.g., $D_{MgO}^{opx/liq} = \%\ MgO_{opx}/\%\ MgO_{liq}$) for MgO between orthopyroxene and liquid as well as between olivine and liquid. The partition coefficients of
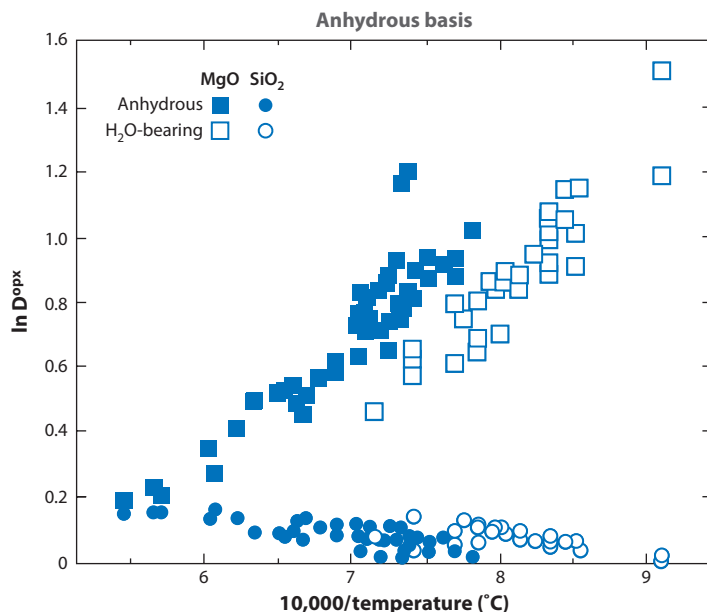
Figure 7

Mineral-melt partition coefficients for orthopyroxene (D^{opx}) in anhydrous (*solid symbols*) and H_2O-bearing (*open symbols*) melts of mantle peridotite. The H_2O-bearing melt compositions are recalculated on an anhydrous basis. The partition coefficient for MgO increases as temperature decreases, but the D for SiO_2 remains constant. The consequence is that lower temperature melts have higher SiO_2. After Parman & Grove (2004).

both minerals are strongly temperature dependent, with D increasing dramatically as T decreases (**Figure 7**) and the presence of H_2O broadening the temperature range of silicate liquid stability to much lower temperatures. However, the D for SiO_2 remains constant, showing only a small temperature dependency. Therefore, mantle lherzolite melts become enriched in SiO_2 because the presence of high amounts of dissolved H_2O lowers the melting temperatures of the mantle.

This effect can be observed in the compositions of natural arc magmas compiled in **Table 1** and in the covariations in temperature, H_2O content, and SiO_2 content (**Figure 8**). Both anhydrous and hydrous basaltic liquids are in equilibrium with their mantle source at high temperatures, but higher SiO_2 primitive arc magmas are higher in H_2O. Melting extent and mantle temperature also play a role, and the boninite compositions included in this data set reflect the effects of high-temperature high-extent hydrous melting. The results of peridotite melting experiments at 0.75 to 2 GPa in the presence of excess H_2O exemplify these effects (Kushiro 1972, Grove et al. 2006, Till et al. 2011) and contain near solidus melts with >12 wt% H_2O at 57 to 60 wt% SiO_2.

EFFECTS OF FRACTIONAL CRYSTALLIZATION

The FeO*/MgO versus SiO_2 diagram was introduced by Miyashiro (1974), who used it to discriminate arc (calc-alkaline) from tholeiitic differentiation trends and to distinguish among different types of calc-alkaline trends that he observed in arcs in the Pacific Ring of Fire. On the Miyashiro (1974) diagram, an anhydrous fractional crystallization trend (tholeiitic trend) is nearly vertical, with FeO*/MgO increasing continuously at constant SiO_2. The differentiation trend followed during fractional crystallization of Galapagos mid-ocean ridge lavas (Grove & Kinzler 1986,

Boninite: An arc-related volcanic rock containing both high SiO_2 (>53 wt.%), high MgO (>8 wt.%) and low TiO_2 (<0.5 wt.%) typically formed during the early stages of subduction in the fore-arc environment
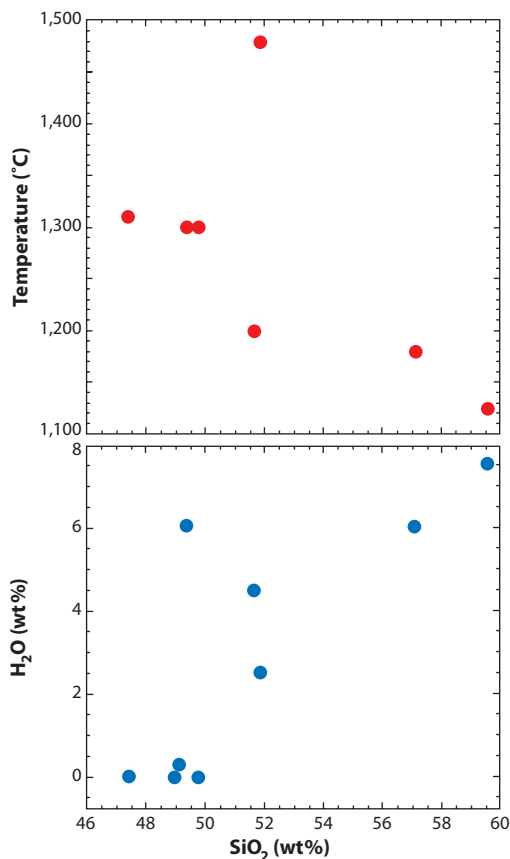
Figure 8

Variations in temperature of mantle melting and in the SiO_2 and H_2O compositions of the near-primary arc mantle melts from **Table 1**. Abbreviation: wt%, weight percent.

Juster et al. 1989) provides an excellent example of a dry tholeiitic trend (**Figure 9b**). Sisson & Grove (1993a) provided the first experimental evidence that liquids produced by crystallization of hydrous basaltic magmas define crystallization paths similar to those found in many calc-alkaline suites, and these lead to high-SiO_2 andesitic residual liquids. The trends illustrated in **Figure 9** are generated in H_2O-saturated experiments carried out at 200 MPa with ∼6 wt% H_2O in the melt (equivalent to a depth of 6 km in the crust and typical conditions for fractional crystallization of calc-alkaline magmas). Under these conditions, H_2O has a significant effect on the mineral phase stability and crystallization sequence and, therefore, on the compositional evolution of liquids produced during fractional crystallization. The major effect of H_2O is to suppress the crystallization of plagioclase and put Fe-Mg-rich silicates on the liquidus. The presence of H_2O also lowers the temperature at which the silicate minerals crystallize, but it has little effect on the temperature at which spinel appears. For example, an iron-rich spinel appears at or near the liquidus of a hydrous basaltic melt (Sisson & Grove 1993a). When late-appearing plagioclase crystallizes, it is rich in calcium and aluminum, which further promotes enrichment of SiO_2 and alkalis in the residual liquids. Therefore, liquids produced by fractional crystallization become depleted in FeO and enriched in SiO_2 to produce the calc-alkaline differentiation trend.
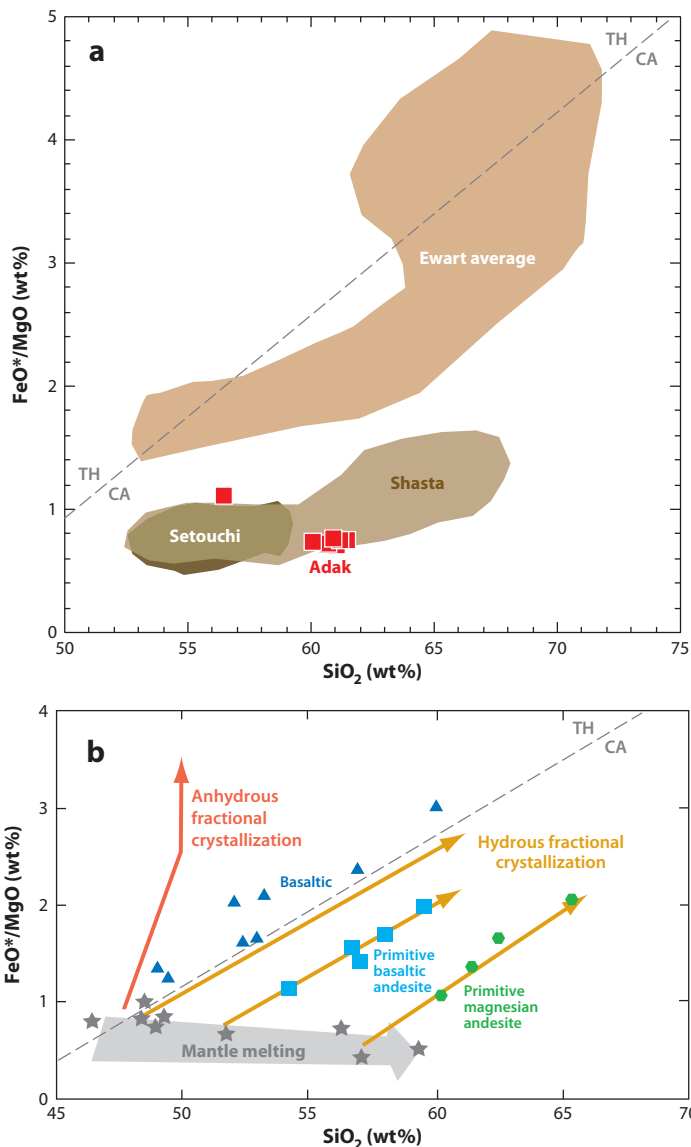
Figure 9

Variation diagrams showing FeO*/MgO versus SiO_2 [all in weight percent (wt%)] and the calc-alkaline (CA) and tholeiitic (TH) dividing line of Miyashiro (1974). FeO* implies that all of the iron in the melt is calculated as divalent iron. (*a*) The compositional range of the global average of arc lava suites compiled by Ewart (1979, 1982) and suites of low FeO*/MgO from Mt. Shasta, California; the Miocene Setouchi volcanic belt, Japan; and Adak Island in the Aleutians (*red squares*). (*b*) The primary mantle melts from **Table 1** (*gray stars*) define the mantle melting array for global arc suites. This trend extends from low-SiO_2 melts in equilibrium with a lherzolite mantle residue (olivine + orthopyroxene + high-Ca pyroxene + spinel) to high-SiO_2, high-degree melts in equilibrium with an harzburgite residue (olivine + orthopyroxene). Also shown is the low-pressure fractional crystallization trend followed under anhydrous conditions from Juster et al. (1989). The contrasting path for fractional crystallization in H_2O-bearing magma suites (hydrous fractional crystallization) is shown for three different starting compositions: basaltic, primitive basaltic andesite, and a primitive magnesian andesite. Modified after Grove et al. (2003).

The majority of arc magmas erupted on Earth today (i.e., Ewart's average arc magmas) (**Figure 9**) follow differentiation trends on the FeO^*/MgO versus SiO_2 diagram that straddle the dividing line between calc-alkaline and tholeiitic, including the Mariana arc, one of Earth's longest arcs. Also shown in **Figure 9a** are the differentiation trends delineated by the two primitive lavas from the Mt. Shasta, California, region (**Table 1**). These primary arc magmas lie in a portion of the FeO^*/MgO versus SiO_2 diagram that is not as commonly represented by modern arc environments. The compositions of the lavas from the Mt. Shasta region along with other arc centers, such as the Aleutians in Alaska (Kay 1980, Yogodzinski et al. 1995), the Setouchi volcanic belt in the SW Japan arc (Tatsumi & Ishizaka 1983, Shimoda et al. 1998), and the Chilean arc (Stern & Kilian, 1996) all display higher SiO_2 at lower FeO^*/MgO. These lavas represent low temperature, high-H_2O content, and high-extent melts of the mantle. In addition, their differentiation trends parallel those of the hydrous basaltic melts, but at lower values of FeO^*/MgO. Despite the fact that these compositions are not commonly found in modern arc environments, they represent an important magma type, as many Archean TTG (tonalite-trondhjemite-granodiorite) suites plot in the same portion of the Miyashiro (1974) diagram. Mechanisms that lead to SiO_2 enrichment in these near-primary magmas are not yet understood and represent an area of active research (Wood & Turner 2009).

HOW MUCH WATER DO SUBDUCTION ZONE MAGMAS CONTAIN?

Determining the pre-eruptive H_2O content of a silicate melt from its solidified product remains a challenging task. The solubility of H_2O is strongly pressure dependent and drops to near zero at atmospheric pressure. Thus, hydrous melts tend to degas as they ascend to the surface. There are several methods for estimating pre-eruptive magmatic H_2O contents (for a review, see Johnson et al. 1994): indirect measurements using mineral/melt equilibria (Sisson & Grove 1993b), direct measurements of liquids trapped in melt inclusions in minerals (Anderson 1974, Sisson & Layne 1993, Wallace 2005), and estimates of water contents from phase equilibria and/or phenocryst assemblage stability (Moore & Carmichael 1998, Carmichael 2002, Rutherford et al. 1985, Krawczynski et al. 2012). Combined evidence from melt inclusions, phase equilibria, and phenocryst assemblage stability has also been used to track the pre-eruptive history of magma recharge, ascent, and residence in long-lived volcanic systems (Blundy et al. 2006, Schmidt & Grunder, 2011, Johnson et al. 2010). Most of the H_2O estimates listed in **Table 1** were obtained using the phase equilibrium method or from measurements of H_2O in melt inclusions. Each of these methods is independent, and together, they record a range of H_2O contents in arc magmas from 0 to 6–7 wt% H_2O (**Figure 10**). The value of 6–7 wt% corresponds to vapor saturation of a basaltic magma at relatively shallow depths (6–8 km). This value could indicate that magmas are degassed and originally contained more H_2O but stalled in a shallow magma chamber.

Thus, still unanswered is the question of the maximum water content present in a subduction zone magma when it last equilibrates with the mantle. The maximum amount of H_2O that can be incorporated during hydrous flux melting depends on the melt production rate in the mantle wedge and on the temperature structure of the wedge. Above, we proposed that the first melts of the hydrous mantle, derived at the cool base of the wedge, are H_2O saturated and subsequently ascend into the hotter, shallower overlying wedge where reactive porous flow dilutes the H_2O in the melt and increases the melting extent. Carmichael (2002) proposed that primary mantle–derived andesite magmas in the Mexican volcanic belt could contain 10 wt% H_2O. Evolved andesites and dacite lavas at Mt. Shasta contain melt inclusions with >10 wt% H_2O (Grove et al. 2003), and McCanta et al. (2007) infer 8 wt% H_2O in the Black Butte dacite. Krawczynski (2011) collected quenched magmatic inclusions from the Mt. Shasta stratocone and from satellite
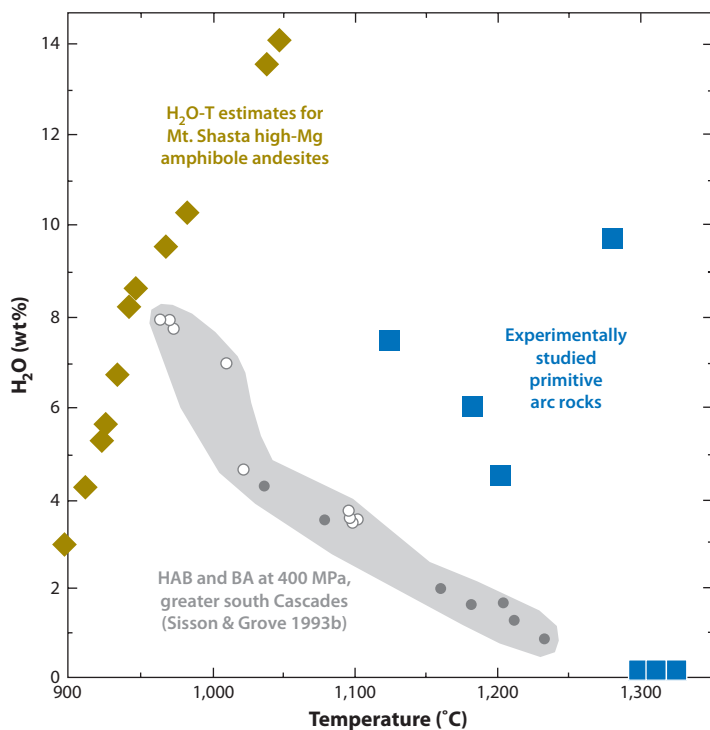
Figure 10

Temperature and H_2O contents of the near-primary arc magmas in their mantle source region from **Table 1** (*dark blue squares*) and pre-eruptive temperature and H_2O contents from mineral melt equilibria for crystallization in the continental crust and uppermost mantle. Porphyritic (*open circles*) and aphanitic lavas (*filled circles*) from the south Cascades region (Sisson & Grove 1993b) are shown in the gray field and highlight the range of H_2O contents in basaltic melts that crystallize at shallow crustal pressures. The dark yellow diamonds (Krawczynski et al. 2012) represent H_2O-saturated melts of andesite that crystallized in a magmatic crystal mush column below Mt. Shasta, California, that extends to mantle depths. A challenge is to understand the conditions that lead to the development of the high-H_2O–low-temperature melts near the mantle-crust transition below some arc volcanoes. Abbreviations: BA, basaltic andesite, HAB, high-alumina olivine tholeiite; wt%, weight percent.

vents and found that primitive mantle melts were emplaced into the Mt. Shasta plumbing system with ~14 wt% H_2O (~800 MPa H_2O saturated) and subsequently crystallized and degassed as they ascended through the crust (**Figure 10**). The Mt. Shasta inclusions contain the assemblage of high Mg# pargasitic amphibole + olivine + pyroxene that requires high H_2O pressures to stabilize it on the liquidus; Krawczynski et al. (2012) reproduced this liquidus assemblage in H_2O-saturated experiments on Mt. Shasta andesite liquids that are in equilibrium with mantle peridotite. Ridolfi et al. (2010) found similarly high pressures and H_2O contents preserved in the phenocryst assemblages in andesite and dacite lavas from Mt. St. Helens, Washington; Soufriere Hills, West Indies; Redoubt, Alaska; and El Reventador, Ecuador.

Also plotted in **Figure 10** are the temperature and H_2O contents inferred for the primitive arc magmas from **Table 1**. These liquids plot at higher temperatures and span the water contents estimated from more evolved arc basalts. The trend of the primitive arc magmas extends up to 7.5 wt%. If we extend the trend to the maximum water contents calculated for the Mt. Shasta inclusions, several of which are primitive magmas, we infer that primitive arc magmas could contain

Primitive magma: the most compatible element-rich compositions in a given suite; refers to near-primary magmas

up to 14 wt% H_2O when separated at the top of the mantle wedge. Mantle melts with higher H_2O contents could form by reactive crystallization at the upper colder portion of the mantle wedge where temperature decreases with decreasing depth. Alternatively, water input into the mantle wedge may be a variable process, and these relatively cold but very high H_2O content rocks reflect ascent paths through a colder part of the wedge (i.e., on the forearc side of path B, **Figure 6**) and thus experienced variable wedge flux melting. The positive sloping trend in H_2O content and temperature shown for the Mt. Shasta inclusions in **Figure 10** likely records continual vapor saturation of the highest water content magmas as they ascend through a crystal mush column prior to eruption from the Mt. Shasta stratocone (Krawczynski 2011).

THE LOCATION OF ARC VOLCANOES

The classic view of the localization of volcanic arcs is that they occur where the depth to the slab–mantle wedge boundary is 110 ± 20 km (Jarrard 1986). Several recent studies provide excellent global compilations regarding the locations of arc volcanoes and the corresponding plate tectonic observables (i.e., convergence rate, slab dip, slab age, etc.) that can be examined for systematic variations (England et al. 2004, Syracuse & Abers 2006). These global compilations demonstrate that the positions of volcanoes in arcs vary in relation to the plate tectonic observables. England & Katz (2010a, 2010b) used these observations to suggest a model where arc volcanoes are located above the place in the mantle wedge where the anhydrous peridotite solidus makes its closest approach to the trench. However, the petrologic constraints on hydrous magma generation at volcanic arcs discussed in this paper, including the H_2O content of arc magmas, the effects of H_2O on basaltic-andesitic phase equilibria, the P-T conditions of hydrous mineral breakdown in the subducting lithosphere, and the P-T conditions of the H_2O-saturated solidus, all suggest H_2O plays a critical role in the generation of primitive arc magmas. Grove et al. (2009) proposed that the locations of arc volcanoes in these global compilations are the result of the interplay between the location of H_2O-rich fluid release from hydrous minerals in the subducted oceanic lithosphere and the temperature of the mantle wedge above this region of fluid release.

Specifically, the interactions of the petrologic variables (e.g., the P-T slope of the vapor-saturated peridotite solidus and hydrous mineral breakdown) with the plate tectonic variables (i.e., slab dip and convergence rate) appear to control the locations of volcanoes above subduction zones, rather than a uniform depth to the slab (**Figure 11**). As shown in **Figure 6**, melting in the mantle wedge can initiate just above the slab over a range of depths (illustrated between paths A and C, **Figure 6a**). Recall that not all these initial melts will evolve in a way that leads to extensive melting and eruption from an arc volcano on Earth's surface. Melts produced from H_2O-saturated melting at path A will likely freeze as soon as they ascend into the cooler overlying mantle (**Figure 6a**). Where the overlying mantle is higher in temperature (e.g., path B, **Figure 6a**), the initial H_2O-rich melts formed at the slab-wedge interface can ascend and continue to melt the mantle by flux melting at H_2O-undersaturated conditions (Grove et al. 2006). These melts then become hot enough and of sufficient volume to ascend through the shallower, cooler part of the mantle and crust and erupt at arc volcanoes. Path C marks the termination of H_2O-rich fluid supply from the breakdown of chlorite and/or serpentine, which will cut off H_2O-saturated melting in the mantle wedge. Between paths B and C, the overlying mantle will be hot enough to allow flux melting to produce hot H_2O-undersaturated melts in the shallower hot core of the mantle wedge that can feed the growth of arc volcanoes on Earth's surface.

Grove et al. (2009) undertook numerical simulations where slab dip (32–64°) and convergence rate (20–100 mm/year), which are observed to vary in subduction zones globally, are used to estimate the depth and temperature at the slab-wedge interface. These models were used to assess
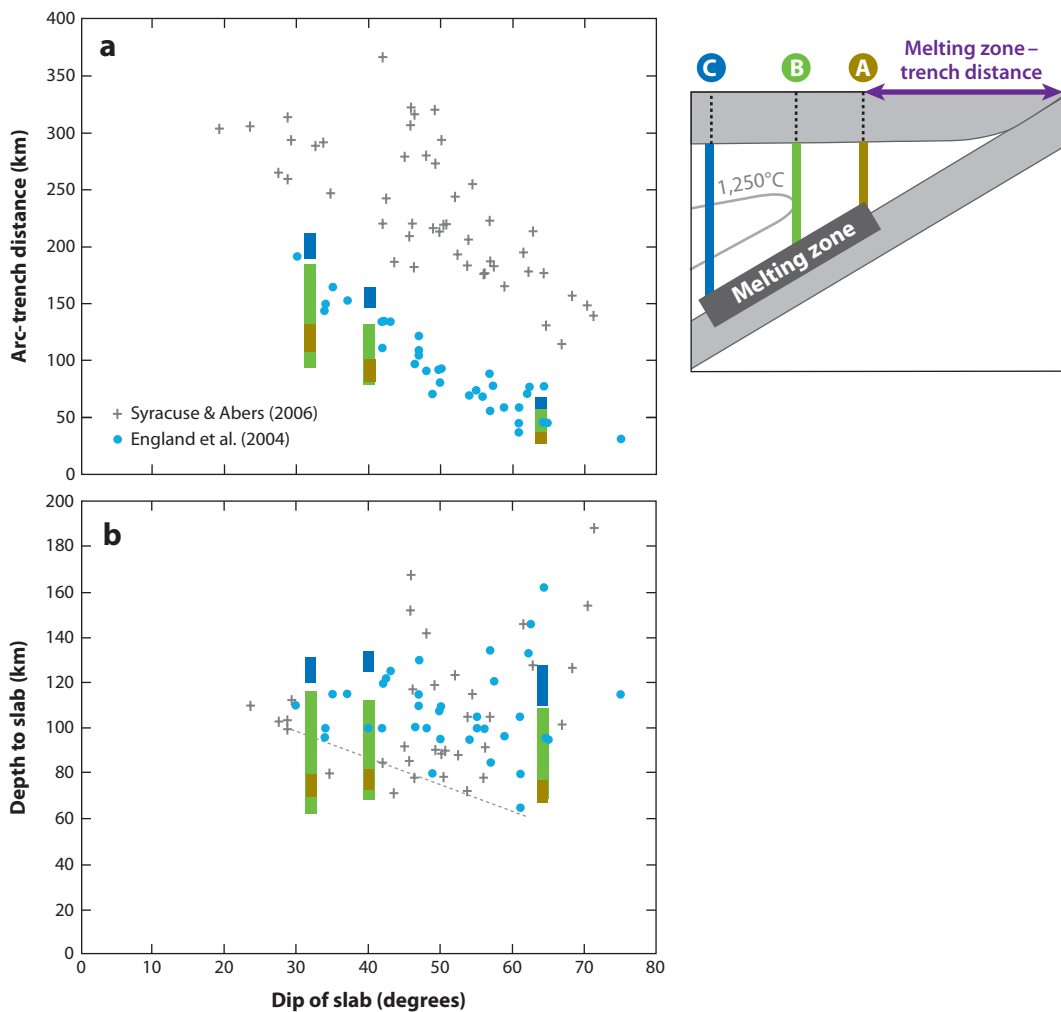
Figure 11

The relationship between the plate tectonic variables at global arcs including (*a*) dip of slab plotted against arc-trench distance (modified from Grove et al. 2010) and (*b*) dip of slab plotted against depth to slab beneath the volcanic front and the corresponding predictions from the numerical models of Grove et al. (2009). The location of volcanoes globally in arc systems can be explained by the interplay of the petrologic variables (e.g., temperature of the H_2O-saturated solidus, pressure-temperature conditions of hydrous mineral breakdown) and the plate tectonic variables at subduction zones (e.g., slab dip, convergence rate), as exemplified by Paths A–C from **Figure 6**. Dashed line in panel *b* illustrates the role slab dip may play in locating the shallowest depth of melting beneath arc volcanoes. Volcanoes that form by hydrous flux melting should plot between paths A and C in **Figure 6**.

the best fit geometry of the A to C region at global subduction zones where the P-T conditions are above the H_2O-saturated solidus and within chlorite stability, thus providing the supply of H_2O to trigger melting at the H_2O-saturated solidus (P,T_{melt} in **Figure 6***b*). The models assume that the shallowest depth of melting, as intersected by path A, is at the low-pressure intersection of chlorite stability and the H_2O-saturated solidus (lowest pressure point in the region of P,T_{melt}). Path B is designated as the vertical path that intersects the nose of the 1250°C isotherm in the models (**Figure 11**). Path C is located at the high-pressure intersection of chlorite stability and

the H_2O-saturated solidus (highest pressure point in the region of P,T_{melt}). When the distance from the trench to the projected intersection of paths A, B, and C with the surface is compared with the observed arc-trench distances from the global subduction data of England et al. (2004), the models match the observed variations reasonably well (**Figure 11a**). Thus the model results illustrate that arc volcanoes form between paths B and C as predicted (where both H_2O supply and temperatures are high). The arc-trench distances in the global compilation of Syracuse & Abers (2006) tend to be 50–100 km greater than those determined by England et al. (2004), which likely stems from systematic differences in how these two studies located the exact position of the trench. In **Figure 11b**, the depth to the slab at paths A, B, and C from the numerical models are compared with the depth to the slab below arc volcanoes determined in the global compilations. The depth to slab below arc volcanoes varies between ~65–70 km and more than 160 km. Slab dip does not appear to be a strong control on the depth to the slab below arc volcanoes, although it may play a greater role in determining the shallowest depth of melting (illustrated by the negative slope of the dashed line in **Figure 11b**). Instead, convergence rate likely plays a role in the positions
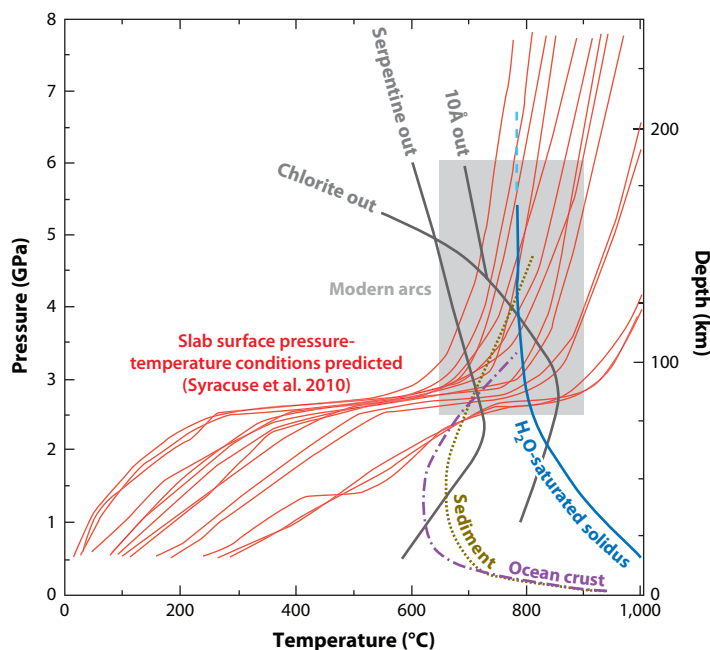
Figure 12

Pressure-temperature (P-T) diagram showing the temperature at the slab-wedge interface predicted by numerical models of Syracuse et al. (2010) for the assumption of full coupling between the slab and the mantle wedge at 80-km depth. Illustrated are the range of slab surface P-T conditions predicted by the models of Syracuse et al. (2010) (*red lines*) and the P-T conditions determined for the slab-wedge interface below modern arcs (*gray box*). The H_2O-saturated peridotite solidus (*blue curve*) and hydrous phase stability fields (*dark gray curves*) from **Figure 6** are superimposed on the models along with the experimentally determined melting curve for H_2O-saturated ocean crust (Liu et al. 1996) (*purple curve*) and sediment (Nichols et al. 1994) (*dark yellow curve*). Also superimposed on this plot are the phase relations for hydrous fertile peridotite from **Figure 4** showing chlorite dehydration, the H_2O-saturated peridotite solidus, and the H_2O-saturated solidi for sediment and basaltic oceanic crust. The H_2O-saturated melting curves and hydrous-phase breakdown reactions for H_2O-rich mantle minerals overlap with the thermal model estimates of the conditions at the base of the mantle wedge and interface with the subducted oceanic lithosphere. We suggest that this leads to the initiation of hydrous flux melting.

of arc volcanoes and paths A, B, and C, as the distance of any given isotherm from the trench decreases with increasing convergence rate. Thus, convergence rate appears to play a greater role in the location of arc volcanoes, and slab dip plays a greater role in determining the location where melting begins in the mantle wedge closest to the trench.

The recent geodynamic models of Syracuse et al. (2010) also predict the thermal structure of the mantle wedge–subducted lithosphere interface. Their models show how the temperature structure for the global range of plate tectonic variables observed in arcs is influenced for different assumptions of the nature of the coupling between the slab and mantle wedge. **Figure 12** shows the results of one of their models in which full coupling between the slab and wedge occurs at 80-km depth. The plate tectonic variables that characterize each arc in their data set are used to calculate a temperature-depth profile for the surface of the subducting slab at that arc. The coincidence of the slab surface temperature with the vapor-saturated solidus and chlorite breakdown for the majority of the models supports the notions that H_2O-saturated peridotite melting can be triggered near the slab-wedge interface and that it happens at a depth in the mantle that coincides with the depth to the slab-wedge interface observed below arcs.

SUMMARY POINTS

1. Near-primary magmas are erupted in many arcs worldwide and require H_2O contents that range from 0 to 7.5 wt% to be in equilibrium with a lherzolite or harzburgite assemblage at their liquidi.

2. P-T estimates from metamorphic rocks and thermal models agree that the slab-wedge interface is ~700–900°C beneath the volcanic zones at arcs. These temperatures put critical constraints on the stability, or lack thereof, of hydrous minerals at the location of H_2O release in the mantle wedge.

3. Small amounts of H_2O given off by the subducting slab lower the melting point of peridotite to between 800 and 820°C at 3 GPa. As the initially H_2O-saturated melt ascends in the wedge, it constantly dissolves silicate material by reactive flux melting in a process that increases the melting extent and dilutes the H_2O content of the melt.

4. The process of reactive flux melting, combined with adiabatic decompression and other possible melting and crystallization processes in the mantle wedge, creates a spectrum of near-primary melts injected into the crustal plumbing systems at arc volcanoes. These melts range from dry olivine tholeiites to hydrous andesites with Mg#s in excess of 0.7.

5. Arc magmas have distinct chemical variations as they crystallize owing to the presence of H_2O. The distinctive enrichment of SiO_2 in these magmas is created by the early crystallization of olivine, pyroxene and amphibole. In addition, the crystallization of plagioclase is suppressed at mid- to lower crustal pressures in H_2O-rich magmas. When it appears the plagioclase is high-Ca and high-Al. Phase equilibria and melt inclusion studies suggest that magmas with 6–8 wt% H_2O are common in the crust, and upper limits of pre-eruptive H_2O contents of magmas are ~12–14 wt%.

6. The stability of hydrous minerals in the mantle wedge and the ability for H_2O-rich melts to travel through the mantle wedge are affected by the plate tectonic variables of subduction zones. These constraints together with the temperature structure and mantle-flow patterns beneath arcs can be used to describe the location of arc volcanoes.

FUTURE ISSUES

1. The fate of mantle melts as they enter the cooler, shallower mantle wedge above the hot core of the subduction zone remains uncertain. At present, we lack a clear understanding of the relative roles of advection of heat and melt into this region and their consequences.

2. The nature of the Moho and lithosphere-asthenosphere boundary beneath arcs raises similar questions. Improvements in numerical models, observations of the seismic structure below arcs, and synthesis of the evidence from different disciplines are needed.

3. The observed diversity in near-primary mantle melts in arcs has yet to be adequately explained. Better sampling of the compositional diversity and its spatial distribution in the global arc system and the relation of this compositional variability to the plate tectonic variables may lead to new insights into the evolution of arc magmatic products through geologic history.

4. The nature of material transport from the subducted oceanic lithosphere into the overlying mantle wedge is very poorly constrained. We lack an understanding on the physical controls on this process. Geologic evidence from exhumed arc roots can provide key constraints. Also lacking is an understanding of the most important material transport and chemical reactions that occur between slab and wedge. For example, the influence of variations in H_2O and its spatial distribution in the slab and wedge are largely unknown, as is the relationship of fluid additions to the abundances of fluid-mobile elements in arc magmas.

DISCLOSURE STATEMENT

The authors are not aware of any affiliations, memberships, funding, or financial holdings that might be perceived as affecting the objectivity of this review.

LITERATURE CITED

Anderson AT Jr. 1974. Evidence for a picritic, volatile-rich magma beneath Mt. Shasta, California. *J. Petrol.* 15:243–67

Asimow PD, Hirschmann MM, Stolper EM. 2001. Calculation of peridotite partial melting from thermodynamic models of minerals and melts: IV. Adiabatic decompression and the composition and mean properties of mid-ocean ridge basalts. *J. Petrol.* 42:963–98

Bartels KS, Kinzler RJ, Grove TL. 1991. High pressure phase relations of primitive high-alumina basalts from Medicine Lake volcano, northern California. *Contrib. Mineral. Petrol.* 108:253–70

Blundy J, Cashman K, Humphreys M. 2006. Magma heating by decompression-driven crystallization beneath andesite volcanoes. *Nature* 443:76–80

Bocchio R, De Capitani L, Ottolini L. 2004. New chemical data on the clinopyroxene-garnet pair in the Alpe Arami eclogite, Central Alps, Switzerland. *Can. Mineral.* 42:1205–19

Brenker FE, Brey GP. 1997. Reconstruction of the exhumation path of the Alpe Arami garnet-peridotite body from depths exceeding 160 km. *J. Metamorph. Geol.* 15:581–92

Brouwer FM, Burri T, Engi M, Berger A. 2005. Eclogite relics in the Central Alps: PT-evolution, Lu-Hf ages and implications for formation of tectonic melange zones. *Schweiz. Mineral. Petrogr. Mitt.* 85:147–74

Cagnioncle AM, Parmentier EM, Elkins-Tanton LT. 2007. Effect of solid flow above a subducting slab on water distribution and melting at convergent plate boundaries. *J. Geophys. Res.* 112:B09402

Carmichael ISE. 2002. The andesite aqueduct: perspectives on the evolution of intermediate magmatism in west-central (105–99°W) Mexico. *Contrib. Mineral. Petrol.* 143:641–63

Davies JH, Stevenson DJ. 1992. Physical model of source region of subduction zone volcanics. *J. Geophys. Res.* 97(B2):2037–70

Debari S, Kay SM, Kay RW. 1987. Ultramafic xenoliths from Adagdak Volcano, Adak, Aleutian-Islands, Alaska: deformed igneous cumulates from the Moho of an island arc. *J. Geol.* 95:329–41

DePaolo DJ. 1981. Trace element and isotopic effects of combined wallrock assimilation and fractional crystallization. *Earth Planet. Sci. Lett.* 53:189–202

Draper DS, Johnston AD. 1992. Anhydrous PT phase relations of an Aleutian high-MgO basalt: an investigation of the role of olivine-liquid reaction in the generation of arc high-alumina basalts. *Contrib. Mineral. Petrol.* 112:501–19

Dvir O, Pettke T, Fumagalli P, Kessel R. 2011. Fluids in the peridotite-water system up to 6 GPa and 800°C: new experimental constrains on dehydration reactions. *Contrib. Mineral. Petrol.* 161:829–44

Elkins-Tanton LT, Grove TL, Donnelly-Nolan J. 2001. Hot, shallow mantle melting under the Cascades volcanic arc. *Geology* 29:631–34

Enami M, Mizukami T, Yokoyama K. 2004. Metamorphic evolution of garnet-bearing ultramafic rocks from the Gongen area, Sanbagawa belt, Japan. *J. Metamorph. Geol.* 22:1–15

England P, Engdahl R, Thatcher W. 2004. Systematic variation in the depths of slabs beneath arc volcanoes. *Geophys. J. Int.* 156:377–408

England PC, Katz RF. 2010a. Global systematics of arc volcano position. *Nature* 468:E6–7

England PC, Katz RF. 2010b. Melting above the anhydrous solidus controls the location of volcanic arcs. *Nature* 467:700–4

Evans BW, Trommsdorff V. 1974. Petrogenesis of garnet lherzolite, Cima Di Gagnone, Lepontine Alps. *Am. J. Sci.* 274:274–96

Evans BW, Trommsdorff V. 1983. Fluorine hydroxyl titanian clinohumite in alpine recrystallized garnet peridotite: compositional controls and petrologic significance. *Am. J. Sci.* 283:355–69

Ewart A. 1979. A recent review of the mineralogy and petrology of Tertiary-Recent, dacitic, latitic, rhyolitic and related sialic rocks. In *Trondjhemites, Dacites and Related Rocks*, ed. F Barker, pp. 13–121. Amsterdam: Elsevier

Ewart A. 1982. The mineralogy and petrology of Tertiary-Recent orogenic volcanic rocks: with special reference to andesite-basaltic compositional range. In *Andesites*, ed. R Thorpe, pp. 25–95. New York: Wiley

Falloon TJ, Danyushevsky LV. 2000. Melting of refractory mantle at 1.5, 2 and 2.5 GPa under anhydrous and H_2O-undersaturated conditions: implications for the petrogenesis of high-Ca boninites and the influence of subduction components on mantle melting. *J. Petrol.* 41:257–83

Fumagalli P, Poli S. 2005. Experimentally determined phase relations in hydrous peridotites to 6.5 GPa and their consequences on the dynamics of subduction zones. *J. Petrol.* 46:555–78

Gaetani GA, Grove TL. 1998. The influence of water on melting of mantle peridotite. *Contrib. Mineral. Petrol.* 131:323–46

Gaetani GA, Grove TL. 2003. Experimental constraints on melt generation in the mantle wedge. In *Inside the Subduction Factory*, ed. J Eiler, pp. 107–34. Washington, DC: Am. Geophys. Union

Gill JB. 1981. *Orogenic Andesites and Plate Tectonics*. New York: Springer-Verlag. 390 pp.

Green DH. 1973. Experimental melting studies on a model upper mantle composition at high-pressure under water-saturated and water-undersaturated conditions. *Earth Planet. Sci. Lett.* 19:37–53

Green DH. 1976. Experimental testing of "equilibrium" partial melting of peridotite under water-saturated, high-pressure conditions. *Can. Mineral.* 14:255–68

Green DH, Hibberson WO, Kovacs I, Rosenthal A. 2010. Water and its influence on the lithosphere-asthenosphere boundary. *Nature* 467:448–51

Grove TL, Chatterjee N, Parman SW, Medard E. 2006. The influence of H_2O on mantle wedge melting. *Earth Planet. Sci. Lett.* 249:74–89

Grove TL, Elkins-Tanton LT, Parman SW, Chatterjee N, Muentener O, Gaetani GA. 2003. Fractional crystallization and mantle-melting controls on calc-alkaline differentiation trends. *Contrib. Mineral. Petrol.* 145:515–33

Grove TL, Kinzler RJ. 1986. Petrogenesis of andesites. *Annu. Rev. Earth Planet. Sci.* 14:417–54

Grove TL, Parman SW, Bowring SA, Price RC, Baker MB. 2002. The role of an H_2O-rich fluid component in the generation of primitive basaltic andesites and andesites from the Mt. Shasta region, N California. *Contrib. Mineral. Petrol.* 142:375–96

Grove TL, Till CB, Lev E, Chatterjee N, Medard E. 2009. Kinematic variables and water transport control the formation and location of arc volcanoes. *Nature* 459:694–97

Grove TL, Till CB, Lev E, Chatterjee N, Medard E. 2010. Global systematics of arc volcano position, Grove et al. reply. *Nature* 468:E7–8

Hacker BR, Anderson TB, Johnston S, Kylander-Clark ARC, Peterman ER, et al. 2010. High-temperature deformation during continental-margin subduction and exhumation: the ultrahigh-pressure Western Gneiss Region of Norway. *Tectonophysics* 480:149–71

Hall PS, Kincaid C. 2001. Diapiric flow at subduction zones: a recipe for rapid transport. *Science* 292:2472–75

Hart SR, Zindler A. 1986. In search of a bulk-Earth composition. *Chem. Geol.* 57:247–67

Hesse M, Grove TL. 2003. Absarokites from the western Mexican volcanic belt: constraints on mantle wedge conditions. *Contrib. Mineral. Petrol.* 146:10–27

Hirose K. 1997. Melting experiments on lherzolite KLB-1 under hydrous conditions and generation of high-magnesian andesitic melts. *Geology* 25:42–44

Hirose K, Kawamoto T. 1995. Hydrous partial melting of lherzolite at 1 GPa: the effect of H_2O on the genesis of basaltic magmas. *Earth Planet. Sci. Lett.* 133:463–73

Hodges FN. 1974. The solubility of H_2O in silicate melts. *Carnegie Inst. Wash. Year Book* 73:251–55

Iwamori H. 1998. Transportation of H_2O and melting in subduction zones. *Earth Planet. Sci. Lett.* 160:65–80

Iwamori H. 2007. Transportation of H_2O beneath the Japan arcs and its implications for global water circulation. *Chem. Geol.* 239:182–98

Jarrard RD. 1986. Relations among subduction parameters. *Rev. Geophys.* 24:217–84

Johnson CM, Anderson AT, Rutherford MJ. 1994. Pre-eruptive volatile contents of magmas. In *Volatiles in Magmas*, ed. MR Carroll, JR Holloway, pp. 281–330. Washington, DC: Mineral. Soc. Am.

Johnson ER, Wallace PJ, Cashman KV, Granados HD. 2010. Degassing of volatiles (H_2O, CO_2, S, Cl) during ascent, crystallization, and eruption at mafic monogenetic volcanoes in central Mexico. *J. Volcanol. Geotherm. Res.* 197:225–38

Juster TC, Grove TL, Perfit MR. 1989. Experimental constraints on the generation of FeTi basalts, andesites, and rhyodacites at the Galapagos Spreading Center, 85°W and 95°W. *J. Geophys. Res.* 94(B7):9251–74

Kawakatsu H, Watada S. 2007. Seismic evidence for deep-water transportation in the mantle. *Science* 316:1468–71

Kawamoto T, Holloway JR. 1997. Melting temperature and partial melt chemistry of H_2O-saturated mantle peridotite to 11 gigapascals. *Science* 276:240–43

Kay RW. 1980. Volcanic arc magmas: implications of a melting-mixing model for element recycling in the crust-upper mantle system. *J. Geol.* 88:497–522

Kay RW, Kay SM. 1993. Delamination and delamination magmatism. *Tectonophysics* 219:177–89

Kelemen PB. 1986. Assimilation of ultramafic rock in subduction-related magmatic arcs. *J. Geol.* 94:829–43

Kelemen PB, Johnson KTM, Kinzler RJ, Irving AJ. 1990. High-field-strength element depletions in arc basalts due to mantle magma interaction. *Nature* 345:521–24

Kelemen PB, Rilling JL, Parmentier EM, Mehl L, Hacker BR. 2003. Thermal structure due to solid-state flow in the mantle wedge beneath arcs. In *Inside the Subduction Factory*, ed. J Eiler, pp. 293–311. Washington, DC: Am. Geophys. Union

Klein EM, Langmuir CH. 1987. Global correlations of ocean ridge basalt chemistry and axial depth and crustal thickness. *J. Geophys. Res.* 92:8089–115

Krawczynski MJ. 2011. *Experimental studies of melting and crystallization processes in planetary interiors*. PhD thesis. Mass. Inst. Technol. and Woods Hole Oceanogr. Inst., Mass. 202 pp.

Krawczynski MJ, Grove TL, Behrens H. 2012. Amphibole stability in primitive arc magmas: effects of temperature, H_2O content and oxygen fugacity. *Contrib. Mineral. Petrol.* In press

Kushiro I. 1990. Partial melting of mantle wedge and evolution of island arc crust. *J. Geophys. Res.* 95:15929–39

Kushiro I. 1972. Effect of water on the compositions of magmas formed at high pressures. *J. Petrol.* 13:311–34

Kushiro I, Syono Y, Akimoto S. 1968. Melting of a peridotite nodule at high pressures and high water pressures. *J. Geophys. Res.* 73:6023–29

Liu J, Bohlen SR, Ernst WG. 1996. Stability of hydrous phases in subducting oceanic crust. *Earth Planet. Sci. Lett.* 143:161–71

McCanta MC, Rutherford MJ, Hammer JE. 2007. Pre-eruptive and syn-eruptive conditions in the Black Butte, California dacite: insight into crystallization kinetics in a silicic magma system. *J. Volcanol. Geotherm. Res.* 160:263–84

Medard E, Grove TL. 2006. Early hydrous melting and degassing of the Martian interior. *J. Geophys. Res.* 111:E11003

Medard E, Grove TL. 2008. The effect of H_2O on the olivine liquidus of basaltic melts: experiments and thermodynamic models. *Contrib. Mineral. Petrol.* 155:417–32

Mibe K, Fuji T, Yasuda A. 1999. Control of the location of the volcanic front in island arcs by aqueous fluid connectivity in the mantle wedge. *Nature* 401:259–62

Millhollen GL, Irving AJ, Wyllie PJ. 1974. Melting interval of peridotite with 5.7% water to 30 kilobars. *J. Geol.* 82:575–87

Miyashiro A. 1974. Volcanic rock series in island arcs and active continental margins. *Am. J. Sci.* 274:321–55

Mizukami T, Wallis S. 2005. Structural and petrological constraints on the tectonic evolution of the garnet-lherzolite facies Higashi-akaishi peridotite body, Sanbagawa belt, SW Japan. *Tectonics* 24:TC6012

Moore G, Carmichael ISE. 1998. The hydrous phase equilibria (to 3 kbar) of an andesite and basaltic andesite from western Mexico; constraints on water content and conditions of phenocryst growth. *Contrib. Mineral. Petrol.* 130:304–19

Mori T, Banno S. 1973. Petrology of peridotite and garnet clinopyroxenite of Mt. Higashi-akaishi Mass, Central Shikoku, Japan: subsolidus relation of anhydrous phases. *Contrib. Mineral. Petrol.* 41:301–23

Mysen BO, Boettcher AL. 1975. Melting of a hydrous mantle: I. Phase relations of natural peridotite at high-pressures and temperatures with controlled activities of water, carbon dioxide, and hydrogen. *J. Petrol.* 16:520–48

Nichols GT, Wyllie PJ, Stern CR. 1994. Subduction zone melting of pelagic sediments constrained by melting experiments. *Nature* 371:785–88

Nicholls IA, Ringwood AE. 1972. Production of silica-saturated tholeiitic magmas in island arcs. *Earth Planet. Sci. Lett.* 17:243–46

Nimis P, Trommsdorff V. 2001. Revised thermobarometry of Alpe Arami and other garnet peridotites from the Central Alps. *J. Petrol.* 42:103–15

Nye CJ, Reid MR. 1986. Geochemistry of primary and least fractionated lavas from Okmok Volcano, Central Aleutians: implications for arc magmagenesis. *J. Geophys. Res.* 91(B10):10271–87

Olker B, Altherr R, Paquin J. 2003. Fast exhumation of the ultrahigh-pressure Alpe Arami garnet peridotite (Central Alps, Switzerland): constraints from geospeedometry and thermal modelling. *J. Metamorph. Geol.* 21:395–402

Paquin J, Altherr R. 2001. New constraints on the P-T evolution of the Alpe Arami garnet peridotite body (Central Alps, Switzerland). *J. Petrol.* 42:1119–40

Parman SW, Grove TL. 2004. Harzburgite melting with and without H_2O; experimental data and predictive modeling. *J. Geophys. Res.* 109:1–20

Pawley A. 2003. Chlorite stability in mantle peridotite: the reaction clinochlore+enstatite = forsterite+pyrope+H_2O. *Contrib. Mineral. Petrol.* 144:449–56

Pearce JA, Baker PE, Harvey PK, Luff IW. 1995. Geochemical evidence for subduction fluxes, mantle melting and fractional crystallization beneath the South Sandwich Island arc. *J. Petrol.* 36:1073–109

Pfiffner M, Trommsdorff V. 1998. The high-pressure ultramafic-mafic-carbonate suite of Cima Lunga-Adula, Central Alps: excursions to Cima di Gagnone and Alpe Arami. *Schweiz. Mineral. Petrogr. Mitt.* 78:337–54

Plank T, Langmuir CH. 1988. An evaluation of the global variations in the major element chemistry of arc basalts. *Earth Planet. Sci. Lett.* 90:349–70

Rapp RP, Watson EB. 1995. Dehydration melting of a metabasalt 8–32 kbar: implications for continental growth and crust-mantle recycling. *J. Petrol.* 36:891–931

Ridolfi F, Renzulli A, Puerini M. 2010. Stability and chemical equilibrium of amphibole in calc-alkaline magmas: an overview, new thermobarometric formulations and application to subduction-related volcanoes. *Contrib. Mineral. Petrol.* 160:45–66

Rudnick RL. 1995. Making continental crust. *Nature* 378:571–78

Rudnick RL, Fountain DM. 1995. Nature and composition of the continental crust: a lower crustal perspective. *Rev. Geophys.* 33:267–309

Rushmer T. 1991. Partial melting of two amphibolites: contrasting experimental results under fluid-absent conditions. *Contrib. Mineral. Petrol.* 107:41–59

Rutherford MJ, Sigurdsson H, Carey S, Davis A. 1985. The May 18, 1980, eruption of Mount St. Helens: 1. Melt composition and experimental phase equilibria. *J. Geophys. Res.* 90:2929–47

Schmidt ME, Grunder AL. 2011. Deep mafic roots to arc volcanoes: mafic recharge and differentiation of basaltic andesite at North Sister Volcano, Oregon Cascades. *J. Petrol.* 52:603–41

Schmidt MW, Poli S. 1998. Experimentally based water budgets for dehydrating slabs and consequences for arc magma generation. *Earth Planet. Sci. Lett.* 163:361–79

Sen C, Dunn T. 1994. Dehydration melting of a basaltic composition amphibolite at 1.5 and 2.0 GPa: implications for the origin of adakites. *Contrib. Mineral. Petrol.* 117:394–409

Shimoda G, Tatsumi Y, Nohda S, Ishizaka K, Jahn BM. 1998. Setouchi high-Mg andesites revisited: geochemical evidence for melting of subducting sediments. *Earth Planet. Sci. Lett.* 160:479–92

Sisson TW, Layne GD. 1993. H_2O in basalt and basaltic andesite glass inclusions from four subduction-related volcanoes. *Earth Planet. Sci. Lett.* 117:619–35

Sisson TW, Bronto S. 1998. Evidence for pressure-release melting beneath magmatic arcs from basalt at Galunggung, Indonesia. *Nature* 391:883–86

Sisson TW, Grove TL. 1993a. Experimental investigations of the role of H_2O in calc-alkaline differentiation and subduction zone magmatism. *Contrib. Mineral. Petrol.* 113:143–66

Sisson TW, Grove TL. 1993b. Temperatures and H_2O contents of low-MgO high-alumina basalts. *Contrib. Mineral. Petrol.* 113:167–84

Smith PM, Asimow PD. 2005. Adiabat_1ph: a new public front-end to MELTS, pMELTS, and pHMELTS models. *Geochem. Geophys. Geosyst.* 6:Q02004

Stern CR, Kilian R. 1996. Role of the subducted slab, mantle wedge and continental crust in the generation of adakites from the Andean Austral volcanic zone. *Contrib. Mineral. Petrol.* 123:263–81

Syracuse EM, Abers GA. 2006. Global compilation of variations in slab depth beneath arc volcanoes and implications. *Geochem. Geophys. Geosyst.* 7:Q05017

Syracuse EM, van Keken PE, Abers GA. 2010. The global range of subduction zone thermal models. *Phys. Earth Planet. Inter.* 183:73–90

Tatsumi Y. 1981. Melting experiments on a high-magnesium andesite. *Earth Planet. Sci. Lett.* 54:357–65

Tatsumi Y, Eggins S. 1995. *Subduction Zone Magmatism.* Cambridge, MA: Blackwell Sci.

Tatsumi Y, Ishizaka K. 1982. Origin of high-magnesian andesites in the Setouchi volcanic belt, southwest Japan: I. Petrographical and chemical characteristics. *Earth Planet. Sci. Lett.* 60:293–304

Tatsumi Y, Hamilton DL, Nesbitt RW. 1986. Chemical characteristics of fluid phase released from a subducted lithosphere and origin of arc magmas: evidence from high-pressure experiments and natural rocks. *J. Volcanol. Geotherm. Res.* 29:293–309

Tatsumi Y, Sakuyama M, Fukuyama H. 1983. Generation of arc basalt magmas and thermal structure of the mantle wedge in subduction zones. *J. Geophys. Res.* 88:5815–25

Till CB, Grove TL, Withers AC. 2011. The beginnings of hydrous mantle wedge melting. *Contrib. Mineral. Petrol.* In press, doi: 10.1007/s00410-011-0692-6

Toksoz M, Minear J, Julian B. 1971. Temperature field and geophysical effects of a downgoing slab. *J. Geophys. Res.* 76:1113–38

Ulmer P, Trommsdorff V. 1995. Serpentine stability to mantle depths and subduction-related magmatism. *Science* 268:858–61

van Keken PE, Currie CA, King SD, Behn MD, Cagnioncle AM, et al. 2008. A community benchmark for subduction zone modeling. *Phys. Earth Planet. Inter.* 171:187–97

van Keken PE, Kiefer B, Peacock SM. 2002. High-resolution models of subduction zones: implications for mineral dehydration reactions and the transport of water into the deep mantle. *Geochem. Geophys. Geosyst.* 3:1056

Wada I, Wang K. 2009. Common depth of slab-mantle decoupling: reconciling diversity and uniformity of subduction zones. *Geochem. Geophys. Geosyst.* 10:Q10009

Wallace PJ. 2005. Volatiles in subduction zone magmas: concentrations and fluxes based on melt inclusion and volcanic gas data. *J. Volcanol. Geotherm. Res.* 140:217–40

Wiens DA, Conder JA, Faul UH. 2008. The seismic structure and dynamics of the mantle wedge. *Annu. Rev. Earth Planet. Sci.* 36:421–55

Wood BJ, Turner SP. 2009. Origin of primitive high-Mg andesite: constraints from natural examples and experiments. *Earth Planet. Sci. Lett.* 283:59–66

Wyllie PJ. 1982. Subduction products according to experimental prediction. *Geol. Soc. Am. Bull.* 93:468–76

Yogodzinski GM, Kay RW, Volynets ON, Koloskov AV, Kay SM. 1995. Magnesian andesite in the western Aleutian Komandorksy region: implications for slab melting and processes in the mantle wedge. *Geol. Soc. Am. Bull.* 107:505–19

Zanetti A, Mazzucchelli M, Rivalenti G, Vannucci R. 1999. The Finero phlogopite-peridotite massif: an example of subduction-related metasomatism. *Contrib. Mineral. Petrol.* 134:107–22

Contents

Indexes

Errata

An online log of corrections to *Annual Review of Earth and Planetary Sciences* articles
may be found at http://earth.annualreviews.org

ANNUAL REVIEWS

It's about time. Your time. It's time well spent.

New From Annual Reviews:

Annual Review of Statistics and Its Application

Volume 1 • Online January 2014 • http://statistics.annualreviews.org

Editor: **Stephen E. Fienberg,** *Carnegie Mellon University*

Associate Editors: **Nancy Reid,** *University of Toronto*

Stephen M. Stigler, *University of Chicago*

The *Annual Review of Statistics and Its Application* aims to inform statisticians and quantitative methodologists, as well as all scientists and users of statistics about major methodological advances and the computational tools that allow for their implementation. It will include developments in the field of statistics, including theoretical statistical underpinnings of new methodology, as well as developments in specific application domains such as biostatistics and bioinformatics, economics, machine learning, psychology, sociology, and aspects of the physical sciences.

Complimentary online access to the first volume will be available until January 2015.

Access this and all other Annual Reviews journals via your institution at **www.annualreviews.org.**

ANNUAL REVIEWS | Connect With Our Experts

Tel: 800.523.8635 (US/CAN) | Tel: 650.493.4400 | Fax: 650.424.0910 | Email: service@annualreviews.org